

Viscosity and structure of iron- and aluminum-bearing calcium silicate melts at 1 atm

B. O. MYSEN, D. VIRGO

*Geophysical Laboratory, Carnegie Institution of Washington
Washington, D. C. 20008*

C. M. SCARFE

*Experimental Petrology Laboratory, Department of Geology
University of Alberta, Edmonton, Canada T6G 2E3*

AND D. J. CRONIN

*Center for Materials Science, National Bureau of Standards
Washington, D. C. 20234*

Abstract

The temperature-viscosity relationships of melts in the system CaO-SiO₂-Fe-O have been determined and their values compared with those of similar melt composition with Al³⁺ rather than Fe³⁺ in substitution for Si⁴⁺. The viscosities of iron-bearing melts range between 5 and 15 poise at superliquidus temperatures, and their activation energies of viscous flow between 8 and 50 kcal/mole as a function of Ca/Si, iron content and temperature (in the range 1400-1600°C). Compared with iron-free melts, the melts show a distinct viscosity increase as 5 wt.% Fe₂O₃ is added. Additional ferric iron results in a reversal of this trend. The activation energy of viscous flow decreases with increasing ferric iron content at constant temperature and with increasing temperature at constant iron content. In contrast, published viscosity data of melts in the system CaO-Al₂O₃-SiO₂ show a continuous viscosity increase with increasing Al₂O₃ content. These melts exhibit Arrhenian behavior at superliquidus temperatures.

From ⁵⁷Fe Mössbauer and Raman spectroscopy of the melt compositions it is concluded that Fe³⁺ and Al³⁺ are in tetrahedral coordination in all melts. The Al/(Al + Si) of structural units in the melts is positively correlated with that of the bulk system, whereas for the iron-bearing melts, Fe³⁺/(Fe³⁺ + Si) does not vary with changes in bulk melt Fe³⁺/(Fe³⁺ + Si). Rather, the relative abundance of iron-bearing structural units is positively correlated with Fe³⁺/(Fe³⁺ + Si) of the bulk melt. It is suggested that the differences in viscous behavior of ferric- and aluminum-bearing silicate melts results from these different structural roles of Fe³⁺ and Al³⁺.

Introduction

A description of the relationships between viscous flow of silicate melts and their bulk compositions at different temperatures and pressures is necessary to the understanding of the mechanisms of magma generation, ascent and emplacement. The viscosities of natural magmatic liquids range over several orders of magnitude. Available data show, for example, that the viscosity of simple silicate melts depends on their degree of polymerization¹ (e.g., Lacy,

1968), Al/(Al + Si) (e.g., Riebling, 1964, 1966; Rossin et al., 1964) and the type of network-modifying cations (Bockris et al., 1955).

The iron content may affect the melt viscosity significantly (Rontgen et al., 1960; Cukiermann and Uhlmann, 1974; Klein et al., 1981). Iron is particularly interesting because it may occur both as Fe²⁺ and as Fe³⁺ in magmatic liquids. The structural positions of these two cations differ significantly in the melts. Whereas ferrous iron generally is a network modifier (Mao et al., 1973; Seifert and

¹ Degree of polymerization can be calculated from the bulk composition of a melt provided that there are structural data available with which the tetrahedrally coordinated cations (T cations) can be assigned. Moreover, it must be established whether or not free oxygens (O²⁻ in the sense of Toop and Samis, 1962) exist in the melts. By free oxygen is meant an O²⁻ that is bonded only

to network-modifying cations (e.g., alkali metals or alkaline earths). Oxygen bonded to metal cations that may occur in tetrahedral coordination either in substitution for Si⁴⁺ or as separate complexes is not considered free oxygen. On the basis of a summary of melt structural data, Mysen et al. (1982a,b) and Seifert et al. (1981) concluded that oxygen in melts compositionally relevant

Olesch, 1977; Nolet et al., 1979; Mysen et al., 1980), ferric iron may occur both as a network former and as a network modifier in silicate melts (e.g. Mysen et al., 1980; Dickenson and Hess, 1981; Virgo et al., 1982, 1983).

The degree of polymerization of a silicate melt depends on the $Fe^{3+}/\Sigma Fe$. Because melt viscosity depends on NBO/T (Lacy, 1968), the viscosity of iron-bearing silicate melts may, therefore, be dependent on $Fe^{3+}/\Sigma Fe$. In addition to the well-known dependence on bulk composition and oxygen fugacity (e.g., Sack et al., 1980; Dickenson and Hess, 1981), the $Fe^{3+}/\Sigma Fe$ is a function of both temperature and pressure (e.g., Mysen and Virgo, 1978, 1983; Mysen et al., 1984). The viscosity of iron-bearing silicate liquids may, therefore, exhibit temperature and pressure dependence that can be related to the $Fe^{3+}/\Sigma Fe$ as well as the temperature and pressure dependence of the structural positions of ferric and ferrous iron in silicate melts.

In view of these considerations, a study was conducted of the viscous behavior and melt structure in simple silicate melts in the system CaO-SiO₂-Fe-O. The results were compared with available viscosity and new melt structural data in the system CaO-Al₂O₃-SiO₂ in order to compare the effects of Fe³⁺ and Al³⁺. This system was chosen because the viscous behavior and the structure of the iron-free end-member compositions as well as possible analogues in the system CaO-Al₂O₃-SiO₂ are well known (Kozakevitch, 1960; Bockris et al., 1955; Rossin et al., 1964; Mysen et al., 1982a, 1984). Thus, relationships between the viscous behavior and structure of the iron-bearing liquids may be established.

Experimental methods

Two compositions, SW40 and WL25, on the join CaO-SiO₂ were chosen as base compositions to obtain melts with a large difference in NBO/Si (1.4 and 2.38, respectively). Five and ten wt.% iron oxide as Fe₂O₃ were added to these compositions (SW40F5, WL25F5, SW40F10 and WL25F10, respectively; Table 1). Electron microprobe analyses of individual experimental charges are available from the senior author upon request. In addition, four compositions with 5 and 10 wt.% Al₂O₃ added (SW40A5, WL25A5, SW40A10 and SW40A10; see Table 1) were prepared and quenched from 1550°C for a comparative Raman spectroscopic study of Al³⁺- and Fe³⁺-bearing melts.

The starting mixtures for viscometry of iron-bearing melts were prepared in 650-g batches from reagent-grade Fe₂O₃ and CaCO₃ and purified quartz sand. Bubble- and crystal-free melts were obtained by melting at approximately 100°C above their liquidus temperatures in an SiC-heated furnace for approximately 2 hr

to natural magmatic liquids occurs either as nonbridging (NBO) or bridging (BO) with no evidence for free oxygen. The degree of polymerization of a melt can then be calculated from the atomic proportions derived from a bulk chemical analysis:

$$NBO/T = (20 - 4T)/T = (\Sigma nM_i^{n+})/T, \quad (1)$$

where O and T are the atomic proportions of oxygen and tetrahedrally coordinated cations, and ΣnM_i^{n+} is the sum of network-modifying cations multiplied by their electric charge. This sum is calculated after subtraction of metal cations necessary for charge-balance of T cations such as Al³⁺ or Fe³⁺.

Table 1. Nominal compositions (wt.%) of starting materials

	WL25F5	WL25F10	SW40F5	SW40F10
SiO ₂	45.01	42.64	57.46	54.43
CaO ²	49.99	47.36	37.54	35.57
Fe ₂ O ₃	5.00	10.00	5.00	10.00
NBO/T*	2.11	1.83	1.25	1.08
	WL25A5	WL25A10	SW40F5	SW40F10
SiO ₂	45.01	42.64	57.46	54.43
CaO ²	49.99	47.36	37.54	35.57
Al ₂ O ₃	5.00	10.00	5.00	10.00
NBO/T*	1.99	1.65	1.18	0.97
	WL25	SW70	SW40	CS2
SiO ₂	47.37	55.75	60.48	68.18
CaO ²	52.63	44.25	39.52	31.82
NBO/Si	2.38	1.70	1.40	1.00

*Calculated under the assumption that all iron is Fe³⁺, and Fe³⁺ and Al³⁺ are in tetrahedral coordination. The Ca/Si of these melts is smaller than that for stabilization of free oxygen (Mysen et al., 1982a).

with continuous stirring. Compositions and homogeneity of starting materials and of glasses formed by quenching portions of the liquids after viscosity measurements were verified by electron microprobe analyses. The same quenched samples were also used to determine the $Fe^{3+}/\Sigma Fe$ and to obtain structural information on Fe³⁺ and Fe²⁺ with the aid of ⁵⁷Fe Mössbauer resonant-absorption analyses. In addition, a set of 30-50 mg of both Al- and Fe-containing samples was prepared in an MoSi₂-heated vertical quench furnace. The samples were prepared and quenched from 1550°C for Raman spectroscopic analysis of the materials. All the samples were quenched in water at a rate of approximately 500°C/sec.

The methods of acquisition and analysis of Mössbauer data are similar to those described by Virgo et al. (1983) and Mysen et al. (1984). A comparison of $Fe^{3+}/\Sigma Fe$ obtained by wet-chemical (as described by Sack et al., 1980) and Mössbauer spectroscopic methods is shown in Table 2. The Mössbauer spectroscopic data have an uncertainty of about 5% (relative; see Mysen et al., 1984). Sack et al. (1980) reported a 6% uncertainty in wet-chemical analysis similar to the method used to obtain the data in Table 2. Thus, the redox data obtained with the two methods are in accord within the combined analytical uncertainty.

The Raman spectra were obtained with 1 watt of the 514-nm line of an Ar⁺ ion laser with the automated Raman spectrometer system described by Mysen et al. (1982b) and Seifert et al. (1982). As discussed in detail with several numerical examples in those two papers, the curve-fitting is done on a completely statistical basis. Those and other results (e.g., Mysen et al., 1982a; Mysen and Virgo, 1984) show that Raman spectra of silicate quenched melts are best fitted with Gaussian lines, whereas the Mössbauer spectra were fitted to Lorentzian lines (see Mysen et al., 1984, 1985b) and Virgo and Mysen, 1984, for discussion). The number of lines, as well as their position (frequency), intensity and halfwidth of each line are unconstrained (independent) variables in the fitting routine. The minimization routine of the least-squares (identi-

Table 2. Comparison of $\text{Fe}^{3+}/\Sigma\text{Fe}$ determined by wet-chemical and Mössbauer spectroscopic methods

Sample	Wet chemistry	Mössbauer spectroscopy
001*	0.80 ± 0.05	0.86 ± 0.04
002*	0.88 ± 0.05	0.96 ± 0.05
004*	0.60 ± 0.04	0.65 ± 0.03
010*	0.89 ± 0.05	0.96 ± 0.05
FeAb*	0.75 ± 0.05	0.82 ± 0.04
MV78†	0.68 ± 0.04	0.71 ± 0.04

*Sample provided by Dr. I. S. E. Carmichael, University of California, Berkeley. Redox data are from Mo et al. (1982) and Carmichael (personal communication, 1983). Uncertainty in wet-chemical analyses as quoted by Sack et al. (1980). For bulk chemical analyses, see Table 1 of Mo et al. (1982).

†From Mysen and Virgo (1978). Bulk composition (by weight): $\text{An}_{46}\text{Fo}_{16.2}(\text{SiO}_2)_{29.7}(\text{Fe}_2\text{O}_3)_{8.1}$ (Osborn, personal communication, 1977; as quoted by Mysen and Virgo, 1978).

cal for both the Mössbauer and Raman data) is based on the methods described by Davidone (1959), Powell and Fletcher (1963) and Powell (1964a,b). The fits result in a minimum χ^2 -value and a maximum in residual distribution. The results of the fitting routine are, therefore, completely independent of any structural model or preconceived interpretation of the spectra.

The melt viscosities were measured with a concentric cylinder viscometer. The experimental design is identical with that described by Scarfe et al. (1983). The viscometer was calibrated with National Bureau of Standards lead silicate glass NBS 711. The viscosities are accurate to $\pm 5\%$ and precise to $\pm 1\%$. Measurements were taken at 50°C intervals after stabilization times of 1 hr at each point. The measurements were routinely performed during cooling from 1600°C , but some data were also obtained by heating from lower temperatures. No measurable differences were observed in the viscosities determined along these two thermal paths. The viscosities were independent of rotational speed of the inner cylinder, a result indicating Newtonian behavior of the liquids. Similar conclusions have been reported for most silicate melts of geological interest at temperatures above their liquidus (e.g., Shaw, 1969; Murase and McBirney, 1973; Scarfe, 1973, 1977). All experiments were conducted in equilibrium with air.

Results

Viscosity measurements

Viscosity-temperature-composition relations are shown in Figure 1 and Table 3. These data are compared with those for aluminous analogues reported by Rossin et al. (1964). All viscosities discussed here are for melts at temperatures above their liquidus (Osborn and Muan, 1960a,b).

Distinct differences in the viscous behavior of the aluminous and ferric-bearing samples were observed (Fig. 1). Addition of either Al_2O_3 or Fe_2O_3 to calcium silicate melts results in a viscosity increase relative to the viscosities of the endmember compositions (WL25 and SW40). For Al_2O_3 , the viscosity increases continuously until $\text{CaO}/\text{Al}_2\text{O}_3 = 0.5$ (molar ratio) for both SW40 and WL25

compositions (see Rossin et al., 1964). In the case of Fe_2O_3 , there is an initial viscosity increase with up to 5 wt.% ferric oxide added. Additional Fe_2O_3 results in a viscosity decrease (Fig. 1) although the values remain higher than the iron-free endmember within the Fe_2O_3 -range studied. It is also notable that the relative viscosity increase resulting from addition of Fe_2O_3 is greater for the least polymerized melt (WL25). Moreover, when recalculated on an atomic basis using the measured $\text{Fe}^{3+}/\Sigma\text{Fe}$ -values in Table 3 [the $\text{Fe}^{3+}/(\text{Fe}^{3+} + \text{Si})$ of WL25F10 is approximately equal to the $\text{Al}/(\text{Al} + \text{Si})$ of WL25A5], solution of ferric iron results in a more rapid increase in viscosity than does aluminum. For the most polymerized composition (SW40), the $\log \eta$ vs. $1/T$ lines in the superliquidus region of the iron-bearing melts display a distinct curvature, whereas those of the analogous aluminous and iron-free endmember melts (Rossin et al., 1964; Bockris and Lowe, 1954) do not (Fig.

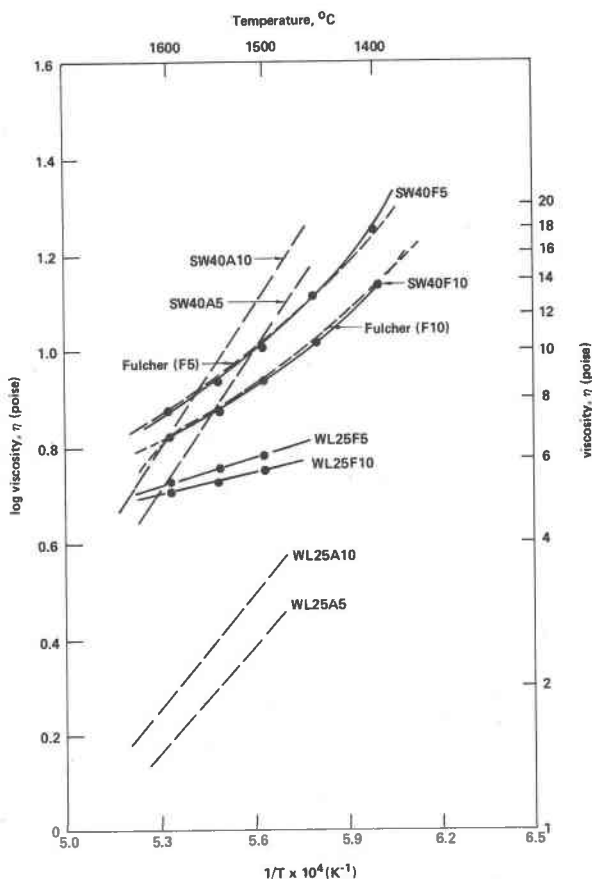


Fig. 1. Temperature-viscosity data of compositions WL25F5, WL25F10, SW40F5 and SW40F10 in the superliquidus temperature regions. Dashed lines labeled WL25A5, WL25A10, SW40A5 and SW40A10 represent viscosity-temperature relations from the analogous aluminous system (data from Rossin et al., 1964). Short-dash lines labeled Fulcher (F5) and Fulcher (F10) are for the least-squares-fitted Fulcher equation (Fulcher, 1925) fitted to the SW40F5 and SW40F10 viscosity data. All liquids were equilibrated with air.

Table 3. Mössbauer spectroscopic and viscosity data

Composition	Temp. °C	Fe ³⁺		Fe ²⁺		Fe ³⁺ /ΣFe	NBO/T [†]	log η
		IS*	QS*	IS	QS			
SW40F10	1600	0.322	1.126	1.031	1.982	0.66	1.24	0.831
SW40F10	1550	0.319	1.161	1.027	1.852	0.68	1.23	0.873
SW40F10	1500	0.312	1.156	1.051	1.976	0.73	1.20	0.935
SW40F10	1450	0.315	1.164	1.045	1.921	0.75	1.19	1.017
SW40F10	1400	0.313	1.156	1.030	1.967	0.82	1.16	1.129
SW40F5	1600	0.330	1.152	1.027	1.952	0.56	1.32	0.875
SW40F5	1550	0.330	1.138	1.027	1.958	0.58	1.32	0.933
SW40F5	1500	0.318	1.110	1.004	1.937	0.67	1.29	1.009
SW40F5	1450	0.356	1.097	1.050	1.928	0.72	1.28	1.115
SW40F5	1400	0.326	1.115	1.195	2.029	0.70	1.28	1.248
WL25F10	1600	0.306	1.197	0.995	2.025	0.79	2.03	0.707
WL25F10	1550	0.331	1.205	1.041	1.987	0.85	1.99	0.727
WL25F10	1500	0.328	1.192	1.032	2.006	0.89	1.95	0.754
WL25F5	1600	0.318	1.192	1.011	2.068	0.69	2.24	0.725
WL25F5	1550	0.329	1.172	1.022	1.995	0.73	2.23	0.747
WL25F5	1500	0.293	1.208	0.970	2.005	0.85	2.18	0.781

*Isomer shift and quadrupole splitting (mm/sec). Isomer shifts are relative to Fe metal.

[†]Calculated as indicated in footnote 1 in text.

1). For the least polymerized composition (WL25), neither data set indicates such curvature within experimental uncertainty, but the temperature dependence of the viscosity of the aluminous samples is much greater than for those that are iron bearing.

Structural studies

The ferric/ferrous and hyperfine parameters (isomer shift, IS, and quadrupole splitting, QS) from the Mössbauer

spectra of quenched melts from the viscosity experiments are shown in Table 3. The Mössbauer spectra of all samples are topologically similar, and only two examples are shown (Fig. 2). The values of the hyperfine parameters, notably the isomer shifts, are insensitive to temperature, Ca/Si, iron content and Fe³⁺/ΣFe in the temperature and composition range studied. Their values are consistent with those commonly observed for crystalline and glassy materials with tetrahedrally coordinated ferric iron and octahedrally coordinated ferrous iron (e.g., Hafner and Huckenholz, 1971; Annersten, 1976; Annersten and Halenius, 1976; Amthauer et al., 1977; Waychunas and Rossman, 1983; Mao et al., 1973; Nolet et al., 1979; Mysen and Virgo, 1983; Mysen et al., 1984) in all iron-bearing melts for which the viscosities were measured.

Additional information on the structural positions of Fe³⁺ as well as Al³⁺ in the WL25A5, WL25A10, SW40A5 and SW40F10 quenched melts may be obtained from their Raman spectra (Fig. 3). Because the distribution of ferric iron and aluminum between coexisting units in the melts may vary with temperature (Mysen et al., 1985a), all samples were quenched at the same rate (500°C/sec) from the same temperature (1550°C). As indicated in Table 3, the iron-bearing WL25 samples have Fe³⁺/ΣFe ranging from 0.69 to 0.89, depending on iron content and temperature. For iron-bearing SW40 melts the range is 0.56–0.82. Thus, the Raman spectra of samples denoted F5 and F10 contain

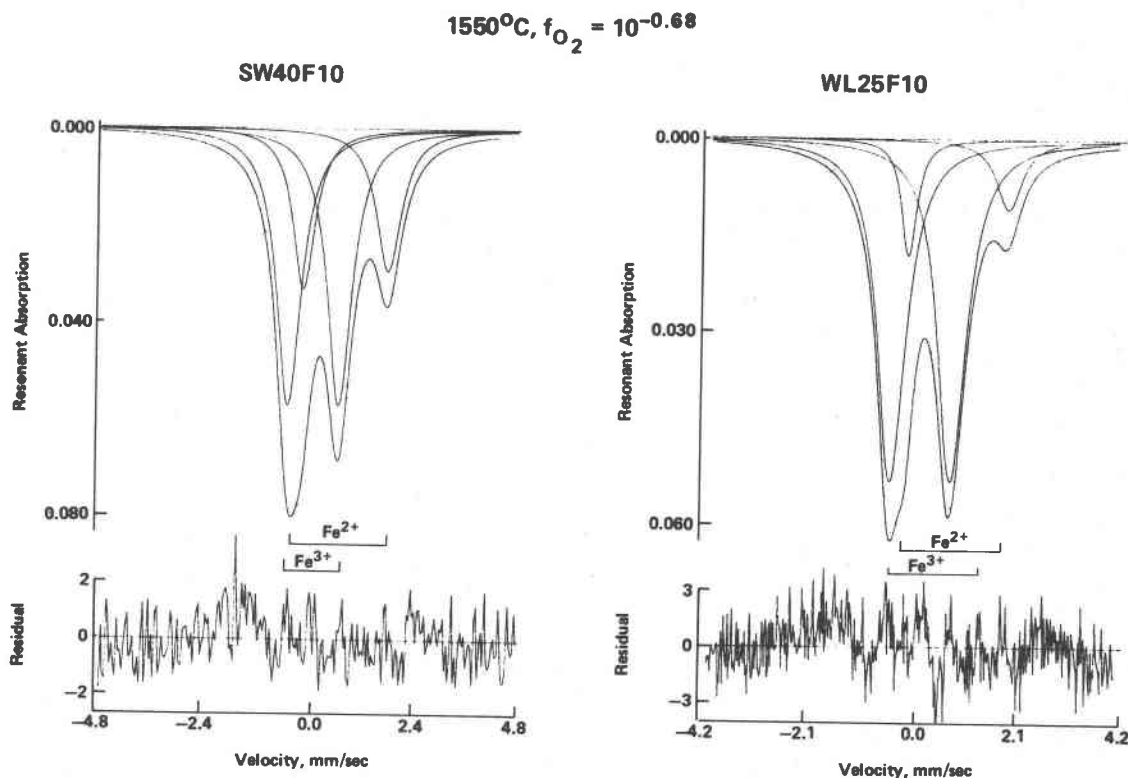


Fig. 2. Representative ⁵⁷Fe Mössbauer resonant spectra of two of the samples used for viscosity measurements (spectra at 298 K).

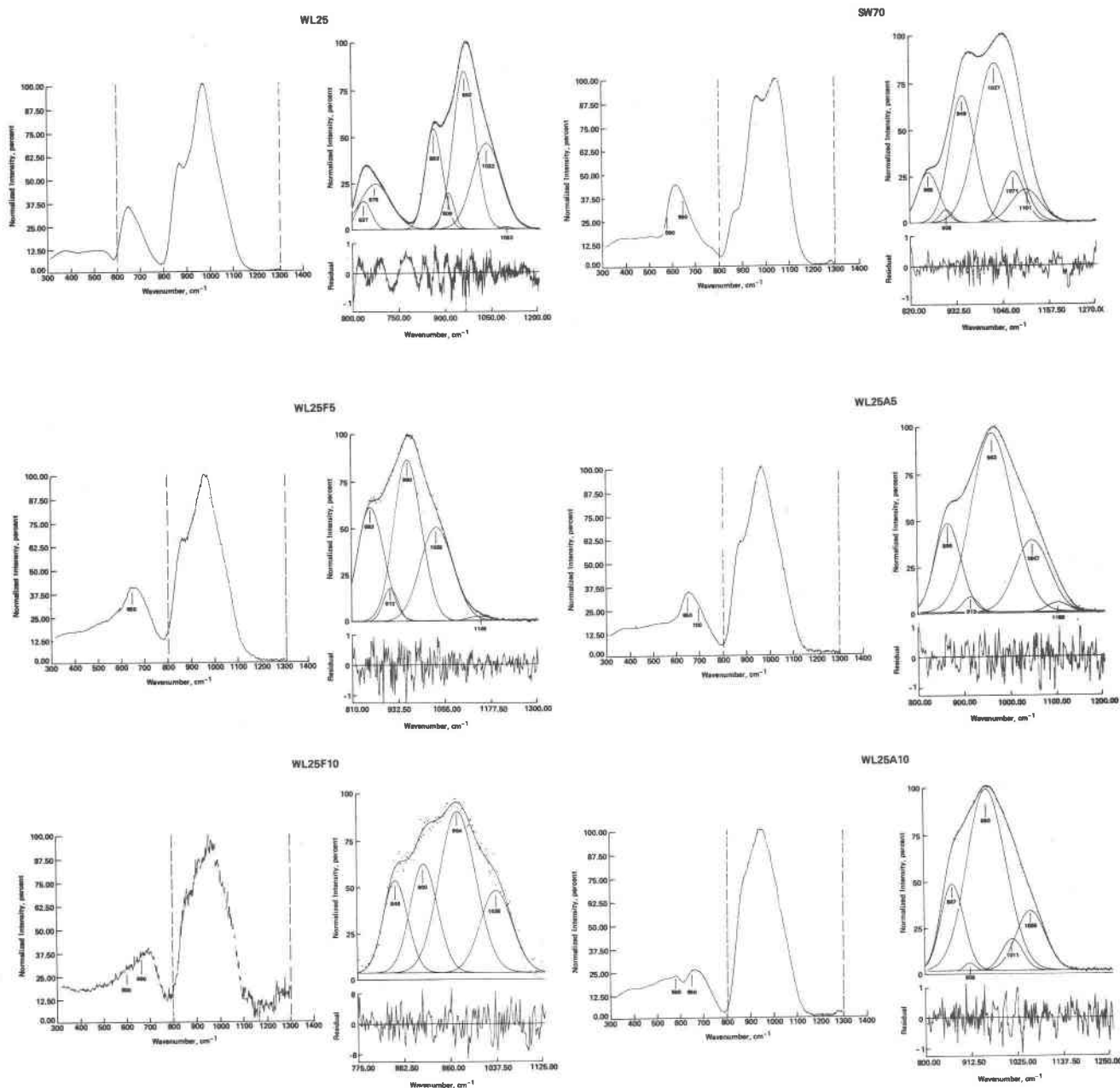


Fig. 3a. Unpolarized, temperature and frequency normalized Raman spectra of depolymerized melts quenched from 1550°C.

a proportion of ferrous iron as shown in Table 3 for samples quenched from 1550°C after equilibration with air.

The addition of tetrahedrally coordinated Fe^{3+} [$\text{Fe}^{3+}(\text{IV})$] or Al^{3+} [$\text{Al}^{3+}(\text{IV})$] to the calcium silicate melts results in polymerization (see Tables 1 and 3). In the most extreme cases, WL25A10 and SW40A10 have NBO/T about 1.65 and 1.0, whereas for the Al-free melts the respective NBO/T values are 2.38 and 1.4 (Table 1). In order to compare the effect on the Raman spectra of such changes

in melt polymerization resulting from Al^{3+} , Fe^{3+} or Si^{4+} , spectra of two additional quenched melts on the join CaO–SiO₂ have been included [CS2 has NBO/Si = 1.0 and SW70 has NBO/Si = 1.7 (from Mysén et al., 1982a)].

The Raman spectra of quenched melts of both WL25 and SW70 contain essentially the same bands (Fig. 3A). Only their relative proportions differ (Table 4). As interpreted by, for example, Verweij (1979a,b), Furukawa et al. (1981), Mysén et al. (1982a), Domine and Piriou (1983) and

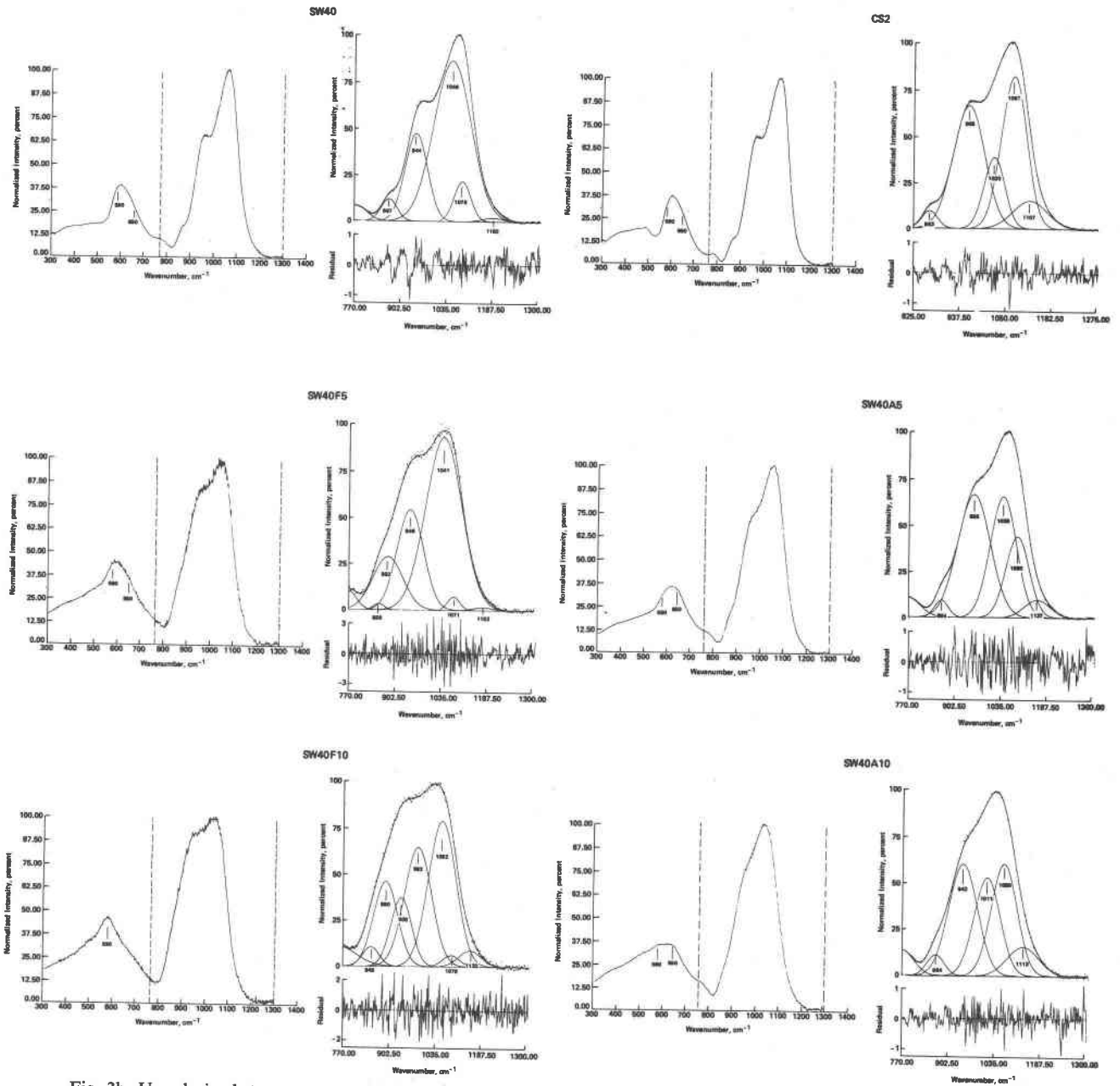


Fig. 3b. Unpolarized, temperature and frequency normalized Raman spectra of polymerized melts quenched from 1550°C.

McMillan and Piriou (1983), the 860-cm^{-1} band results from Si-O^- (O^- , nonbridging oxygen) stretch vibrations in SiO_4^{4-} units. The bands near 910 , 960 and 1070 cm^{-1} represent Si-O^- stretching of bands in $\text{Si}_2\text{O}_6^{6-}$, SiO_3^{2-} and $\text{Si}_2\text{O}_5^{2-}$ units, respectively. In addition, a weak, depolarized band occurs between 1100 and 1150 cm^{-1} (referred to as 1130 cm^{-1} in Table 4). This band is due to Si-O° stretching (O° is a bridging oxygen) in SiO_2 units. The intense band near 1040 cm^{-1} is an Si-O° stretch band involving bridging oxygen in any structural unit (Lasaga, 1982;

Mysen et al., 1982a, 1984). The $\text{Si}_2\text{O}_7^{6-}$ units are also represented by Si-O-Si bending or mixed bending and stretching near 700 cm^{-1} , and the SiO_3^{2-} and $\text{Si}_2\text{O}_5^{2-}$ units, by Si-O-Si bending or bending and stretching motions resulting in Raman bands near 650 and 590 cm^{-1} , respectively. Furukawa et al. (1981) calculated that the frequency of this band is a systematic function of the NBO/Si and the Si-O-Si angle. Their calculated frequencies were 589 cm^{-1} and 654 cm^{-1} for disilicate ($\text{Si}_2\text{O}_5^{2-}$; NBO/Si = 1) and metasilicate (SiO_3^{2-} ; NBO/Si = 2), respectively. For

Table 4. Relative proportions (%) of Si-O [and Fe³⁺(IV)-O] stretch bands in Raman spectra of melts quenched from 1550°C

Composition	NBO/T*	860/EA [†]	960/EA	1070/EA	1130/EA	900/EA
WL25	2.38	33	66	1	-	-
WL25F5	2.23	39	59	-	2	6.4 [‡]
WL25F10	1.99	28	72	-	n.d. [§]	36.8 [‡]
WL25A5	1.98	28	73	2	-	2
WL25A10	1.64	18	65	17	-	1
SW70	1.70	17	50	17	14	2
SW40	1.40	11	64	22	3	-
SW40F5	1.32	2	90	6	2	54 [‡]
SW40F10	1.23	14	62	8	16	231 [‡]
SW40A5	1.18	3	61	29	7	-
SW40A10	0.97	5	44	39	12	-
CS2	1.00	4	44	44	8	-

*Nonbridging oxygen per tetrahedrally coordinated cations calculated with both Al³⁺ and Fe³⁺ in tetrahedral coordination with Fe³⁺/ΣFe from Table 3.

[†]EA is the sum of the areas of Si-O stretch bands. In iron-free samples, this area also includes Si-O⁻ stretching in Si₂O₇⁶⁻ units.

[‡]900 cm⁻¹ considered due to only Fe³⁺(IV)-O stretching.

[§]Not determined. In this composition mass balance requires at least one structural unit with NBO/T ≥ 2. Very low scattering efficiency of this sample resulted, however, in a spectrum whose statistical quality did not warrant inclusion of bands that may stem from such structural units.

||Includes both 900- and 980-cm⁻¹ bands from Fe³⁺(IV)-O stretch bands.

pyrosilicate (Si₂O₇⁶⁻; NBO/Si = 3) the value is near 700 cm⁻¹ (Lazarev, 1972; Tarte et al., 1973). These frequencies are in good agreement with those found here (Fig. 3).

The relative intensities of Raman bands from similar vibrations reflect the relative proportions of the anionic units in the melts. Decreasing NBO/Si (or Ca/Si) in melts along the join CaO-SiO₂ results in decreasing relative abundance of SiO₄⁴⁻ and Si₂O₇⁶⁻ units (Table 4) coupled with an initial increase of SiO₃²⁻ and finally Si₂O₅²⁻ and SiO₂ units (see also the spectra of SW40 and CS2; Fig. 3B and Table 4 and Mysen et al., 1982a; Fig. 10).

The addition of tetrahedrally coordinated ferric iron (with a concomitant increase in melt polymerization; Table 3) is reflected in a new band near 900 cm⁻¹ in the spectra of SW40F5 and SW40F10 quenched melts, and a significant intensity increase in the band near 900 cm⁻¹ in the spectra of WL25F5 and WL25F10 quenched melts. No intensity increase is observed near 700 cm⁻¹ in the spectra of WL25F5 and WL25F10 quenched melts compared with that of iron-free WL25. The frequencies of the Si-O stretch bands seem unaffected. In composition SW40F10 (Fig. 3B), an additional band has appeared near 980 cm⁻¹. Both the 900- and 980-cm⁻¹ bands are interpreted as due to Fe(IV)-O stretching (Fox et al., 1982; Mysen et al., 1980; Virgo et al., 1982), although in these spectra the 900-cm⁻¹ band cannot be distinguished from that of Si-O⁻ stretching in Si₂O₇⁶⁻ units. The absence of an intensity increase near 700 cm⁻¹ in iron-bearing WL25 and the complete absence of a 700 cm⁻¹ band in the spectra of iron-bearing SW40 samples [which would result from Si-O-Si bending or mixed bending and stretching in Si₂O₇⁶⁻ units] leads to the conclusion that the increased 900-cm⁻¹ intensity is primarily due to Fe³⁺(IV)-O stretching and not to Si-O⁻ stretching in Si₂O₇⁶⁻ units. In addition to these changes, in the spectrum of quenched WL25F5 melt the intensity of the

960-cm⁻¹ band (SiO₃²⁻) has decreased and that of the 860-cm⁻¹ band (SiO₄⁴⁻) has increased together with the appearance of a new band near 1130 cm⁻¹ (SiO₂). The relatively poor statistical quality of the spectrum of quenched WL25F10 melt precludes such detailed curve-fitting.

In the aluminous WL25 samples (Fig. 3A), 5 wt.% Al₂O₃ results in a significant intensity increase in the 960-cm⁻¹ band (SiO₃²⁻), a small increase in the 1070-cm⁻¹ band (Si₂O₅²⁻) and significant lowering of the relative intensities of the 860- (SiO₄⁴⁻) and 900-cm⁻¹ (Si₂O₇⁶⁻) bands (Table 4). No evidence for an 1130-cm⁻¹ band (SiO₂ units) was observed. These relative changes are consistent with an overall decrease in NBO/T of these melts as 5 wt.% Al₂O₃ is added. Additional Al₂O₃ is accompanied by further intensity increases of the bands due to SiO₃²⁻, Si₂O₅²⁻ and SiO₂ units together with a lowering of the frequencies of the 1070- and 960-cm⁻¹ bands (to 1055 and 950 cm⁻¹, respectively) as well as a reduction in frequency of the 1030-cm⁻¹ band (to about 1010 cm⁻¹). These frequency changes are responsible for the overall topological differences between the spectra of WL25A10 and SW70 (similar NBO/T but different types of T cations) (Fig. 3A).

Analogous spectroscopic changes occur by the addition of Fe₂O₃ and Al₂O₃ to SW40 melt (Fig. 3B; Table 4). The addition of Fe₂O₃ results in stabilization of Fe³⁺(IV)-oxygen tetrahedral units (900- and 980-cm⁻¹ bands; see also Fox et al., 1982; Virgo et al., 1982; Mysen et al., 1984) with no indication that the Si-O stretch frequencies, only the relative intensities, respond to increasing iron content. With analogous proportions of Al₂O₃ added to SW40 melt, both the relative intensities and the frequencies of the Si-O stretch bands change.

The present data as well as published spectroscopic and other data are consistent with tetrahedrally coordinated Fe³⁺ and Al³⁺ in these melts (see, for example, Taylor and Brown, 1979a,b; Mysen et al., 1981, 1982a,c, 1985a; Fox et al., 1982; Furukawa et al., 1981; Virgo et al., 1982, 1983; Seifert et al., 1982; Navrotsky et al., 1982; McMillan et al., 1982). The increased relative intensities, indicating increases in SiO₃²⁻, Si₂O₅²⁻ and SiO₂ relative abundances in the melts, are consistent with the decrease in bulk melt NBO/T as Fe₂O₃ or Al₂O₃ is added. The frequency decreases with increasing Al³⁺ indicate that Al³⁺ is substituted for Si⁴⁺ in the structural units (as also concluded by Seifert et al., 1982 and Mysen et al., 1982c, 1985a, for compositionally related melts). In those studies (all of which employed statistical curve-fitting methods similar to that used here), it was found that Raman frequencies due to stretch vibrations of T-O bonds (T = Si,Al) decrease as a systematic function of increasing Al/(Al + Si) of TO₂, T₂O₅²⁻ and TO₃²⁻ structural units. An alternative spectroscopic interpretation (McMillan et al., 1982) rests on the a priori assumption that the Al³⁺ in Al-O-Si bridges spectroscopically can be considered similar to network-modifying cations such as alkalis or alkaline earths. The Raman data of McMillan et al. (1982) were deconvoluted (with no description of deconvolution method) to be con-

sistent with this concept. This interpretation of the Raman spectra is, however, inconsistent with the observations from direct comparison of Raman spectra of alkali and alkaline earth silicate melts with those of aluminosilicate melts with tetrahedrally-coordinated Al^{3+} (see also Mysen et al., 1982a, Figs. 4–8 and 11, and Mysen et al., 1985a, Fig. 5, for comparison of relevant spectra of aluminosilicate and alkali and alkaline earth silicate melt spectra). It is also inconsistent with results from molecular orbital calculations (see Mysen et al., 1985a, for detailed discussion). The systematic and continuous frequency decrease with a continuous increase in $Al/(Al + Si)$ is, however, consistent with a systematic decrease in the force-constants for stretching of T–O bonds in aluminosilicate melts (Seifert et al., 1982). The absence of frequency adjustments as Fe^{3+} is added leads to the conclusion that this cation forms separate oxygen complexes (Virgo et al., 1982). The formation of such $Fe^{3+}(IV)$ complexes results in an increased polymerization of the silicate portion of these melts. In general, solution of $Fe^{3+}(IV)$ results in a broader distribution of units with different NBO/Si than is the case for the aluminous analogues.

Discussion

The temperature–viscosity relations at superliquidus temperatures exhibit a distinct curvature of $\log \eta$ vs. $1/T$ at least for the most polymerized iron-bearing melts (Fig. 1). For the depolymerized compositions (WL25F5 and WL25F10), the data may indicate a very slight curvature, but this deviation from linearity is within the 5% relative uncertainty in the viscosity measurements. Thus, a simple Arrhenius equation,

$$\log \eta = \log \eta_0 + E\eta/RT, \quad (2)$$

where R is the gas constant and $\log \eta_0$ is a constant, may be fitted to the data. Similar expressions hold for all the aluminous analogues (Rossin et al., 1964). For the melt compositions SW40F5 and SW40F10, on the other hand, higher order polynomials are required to fit the data. A polynomial of the form

$$\log \eta = a + b(a/T) + c(1/T)^2 \quad (3)$$

can be used to fit the data within 0.002 log unit. The Fulcher equation, $\log \eta = \log \eta_0 + A/B(T - T_0)$ (Fulcher, 1925), commonly used to reproduce nonlinear viscosity–temperature relationships of silicate glasses and melts (see Richet, 1984), results in a fit that reproduces the data within 0.01–0.02 log unit and yields a negative value for T_0 . This result may be at least partly due to the relatively narrow temperature range of the viscosity data. The deviations are particularly significant at the lowest and highest temperatures. The dot-dash curves in Figure 1 represent the least-squares-fitted Fulcher equation. In the current study, equation (3) is used, with the least-squares-fitted coefficients given in Table 5.

Differentiation of equation (3) with respect to $1/T$ yields

Table 5. Regression coefficients for the expression $\log \eta = a + b(1/T) + c(1/T)^2$

Composition	a	b	c
SW40F10	0.1132×10^2	-0.4223×10^5	0.4247×10^8
SW40F5	0.1078×10^2	-0.3941×10^5	0.3894×10^8
WL25F10	-0.2701	0.1860×10^4	-
WL25F5	-0.1214	0.1550×10^4	-
R56*	0.1959×10^2	-0.6624×10^5	0.5696×10^8

*Data from Rontgen *et al.*, (1960)

an expression for the temperature dependence of the activation energy of viscous flow:

$$E\eta = 2.303R[b + 2c(1/T)], \quad (4)$$

where R is the gas constant and the coefficients b and c are from Table 5. Thus, the activation energy of viscous flow of iron-bearing SW40 melts in the superliquidus temperature region is a linear function of $1/T$ (absolute temperature). Qualitatively similar viscous behavior has been observed in the system CaO–FeO–SiO₂ (Rontgen et al., 1956, 1960) and in several alkaline earth-bearing silicate melts (Scarfe et al., 1983; Richet, 1984).

The distinct temperature dependence of $E\eta$ for SW40F5 and SW40F10 melts in the superliquidus temperature range differs from that of the SW40A5 and SW40A10 melts (Rossin et al., 1964) in the same temperature range (Figs. 1 and 4). This observation may be the result of at least three different melt structural factors. (1) The absolute concentrations of ferric and ferrous iron in the melts are temperature dependent. The unusual viscous behavior may be directly related to the abundance of Fe^{3+} - and Fe^{2+} -bearing structural units in the melt. (2) The $Fe^{3+}/\Sigma Fe$ affects the overall bulk melt polymerization (NBO/T). The $E\eta$ depends on the same factor. The $Fe^{3+}/\Sigma Fe$ decreases with increasing temperature thus resulting in increasing NBO/T. This relationship may possibly explain the decreasing $E\eta$ with increasing temperature. (3) The configurational entropy of the melts may depend on the relative proportions of structural units in the melt, where the configurational entropy can be related to activation energy of viscous flow (Richet, 1984). These relative proportions depend on $Fe^{3+}/\Sigma Fe$ and temperature. Therefore, the configurational entropy is temperature- and $Fe^{3+}/\Sigma Fe$ -dependent. These possibilities will be evaluated in turn.

It is possible that the increased concentration of Fe^{2+} and the decrease in Fe^{3+} content with increasing temperature may explain the temperature dependence of the viscosity and activation energy of viscous flow of iron-bearing SW40 melts. This latter suggestion is unlikely, however, because at constant temperature the $E\eta$ of SW40F10 melt is lower than that of SW40F5 melt (Fig. 4) even though the ferric iron content in SW40F10 melt is greater than that of SW40F5 melt (Table 3). For melts in the system

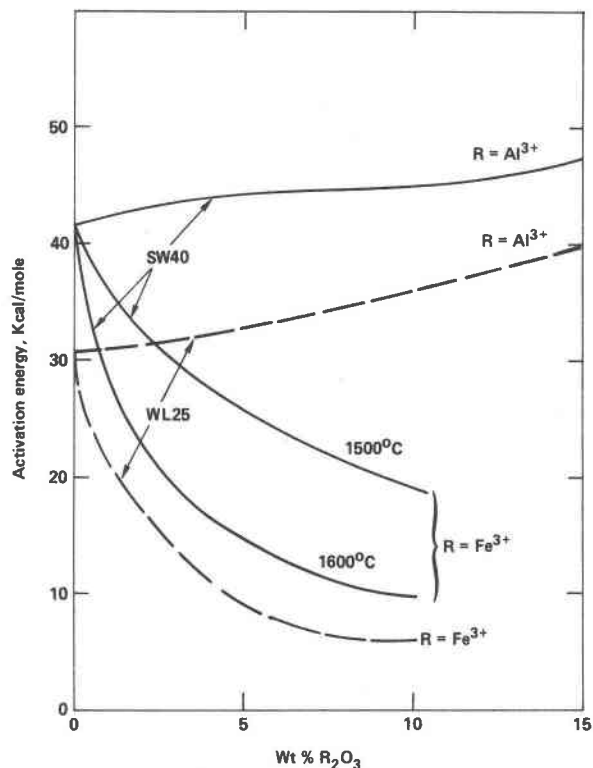


Fig. 4. Activation energies of viscous flow as a function of R_2O_3 (wt.%) added to sample. For compositions SW40F5 and SW40F10, activation energies are temperature dependent, and two representative temperatures (1500°C and 1600°C) are shown.

CaO-FeO-SiO₂ (Rontgen et al., 1960), the curvature in $\log \eta$ vs. $1/T$ is pronounced (see curve R56; Fig. 5) even though these melts contain practically no Fe^{3+} .

Inasmuch as the bulk NBO/T of the iron-bearing melts is slightly temperature dependent ($Fe^{3+}/\Sigma Fe$ decreases and thus NBO/T increases, with increasing temperature; Table 3), one may suggest that the viscosity data fitted to equations (3) and (4) are related to the temperature-dependent $Fe^{3+}/\Sigma Fe$ and, therefore, degree of polymerization of the melts. Both $E\eta$ and η generally decrease in a given chemical system with increasing NBO/T (Lacy, 1968; see also viscosity data on melts on binary metal oxide-silica joins; Kozakevitch, 1960; Bockris and Lowe, 1954; Bockris et al., 1955). The lines labeled "SW40F10", "SW40F5", "WL25F10" and "WL25F5" represent activation energies for viscosity of melts on the binary join CaO-SiO₂ with the same NBO/Si values as those calculated for the iron-bearing SW40 and WL25 melts at the same temperatures. These calculated curves differ distinctly both in slope and relative position from those derived experimentally (Fig. 5). An $Fe^{3+}/\Sigma Fe$ -controlled behavior of $E\eta$ and η is also inconsistent with the observation that for WL25F5 and WL25F10 melts the activation energies are practically in-

dependent of temperature. This is not so for SW40F10 and SW40F5 melts even though the relative change in the degree of polymerization (NBO/T) resulting from the temperature-dependent $Fe^{3+}/\Sigma Fe$ is nearly the same for all the melts (Table 3).

For the melt studied here, it appears, therefore, that an $Fe^{3+}/\Sigma Fe$ -based mechanism is insufficient to explain the magnitude of the temperature-dependent $E\eta$ (see Fig. 5). Furthermore, such a mechanism does not explain the observation that in the concentration range between 5 and 10 wt.% Fe_2O_3 added to the melts, both $E\eta$ and η decrease. As a result of this increased Fe_2O_3 content, the $Fe^{3+}/\Sigma Fe$ increases (at the same temperature) as does the absolute Fe^{3+} -content thus resulting in a lowering of NBO/T of the melt (Table 3). It would be likely that if this were the explanation of the relationship between iron content and viscosity, the viscosity should increase in this iron concentration range (as observed, for example, for added Al_2O_3 ; Rossin et al., 1964), but it does not.

The unusual viscous behavior of iron-bearing melts and the apparent contrast in this behavior between Fe^{3+} and Al^{3+} -bearing liquids may be, at least partly, understood in terms of the configurational entropy theory of Adam and Gibbs (1965) and Richet (1984) in conjunction with the data on melt structure inferred from Figures 2 and 3. According to this theory, the principal expression to relate configurational entropy to the viscosity of silicate melts is (Richet, 1984)

$$\log \eta = \log \eta_0 + Be/TS_{conf} \quad (5)$$

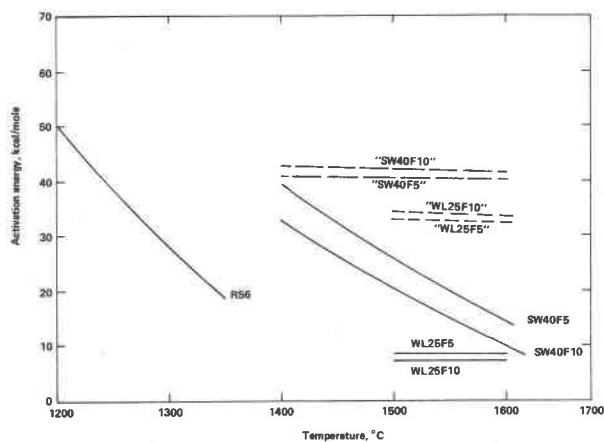


Fig. 5. Temperature dependence of the activation energies of viscous flow for compositions SW40F5 and SW40F10 calculated from equation (4) and compared with that of composition R56 (NBO/T = 2.98; FeO = 20 wt.%) from Rontgen et al., 1960 (composition 56 is their study). The activation energies of compositions WL25F5 and WL25F10 are independent of temperature in the superliquidus temperature region (see text). Notations in quotation marks represent activation energies calculated for CaO-SiO₂ melts with the same NBO/T as those resulting from the $Fe^{3+}/\Sigma Fe$ at given temperature (see text for further discussion).

where S_{conf} is configurational entropy, T is absolute temperature, $\log \eta_0$ and Be are constants. The Be includes the molar free hindrance energy and the configurational entropy of the smallest cooperatively rearranging unit (Adam and Gibbs, 1965). In equation (5), the ratio Be/S_{conf} can be related to the activation energy as

$$E\eta = RBe/S_{\text{conf}}. \quad (6)$$

Thus, the changes in activation energy may be discussed in terms of the configurational entropy of the melts. This term, in turn, may be at least partly related to the types and proportions of coexisting anionic units, X_i , in the melts, where a mixing term of the form $S^{\text{mix}} = -R\sum X_i \ln X_i$ contributes to the total configurational entropy. This term varies with bulk composition at constant temperature (and pressure) and with temperature (and pressure) at constant bulk composition (Mysen et al., 1982a, 1984, 1985a). Changes in activation energy of viscous flow resulting from variations in the $\sum X_i \ln X_i$ term may then be expressed as

$$(E\eta)_a / [(E\eta)_a + (E\eta)_b] = (1/\sum X_i \ln X_i)_a / [(1/\sum X_i \ln X_i)_a + (1/\sum X_i \ln X_i)_b] \quad (7)$$

The relative intensities of the Raman bands in the high-frequency envelopes of the Raman spectra (Fig. 3; Table 4) are positively correlated with the relative abundance of the corresponding anionic units and can be used to estimate the relative abundances, X_i (Seifert et al., 1981; Mysen et al., 1982a). These intensities do, however, depend on the presence of tetrahedrally coordinated cations other than Si^{4+} in substitution for silicon. Thus, for Al-bearing melts where the Raman data indicate that the $\text{Al}/(\text{Al} + \text{Si})$ of each unit is a function of the $\text{Al}/(\text{Al} + \text{Si})$ of the melt system, the proportions of the units cannot be obtained with this method (see Mysen et al., 1982c, 1985a, for further discussion of such problems). In the iron-bearing melts, on the other hand, there is no evidence for a continuous change in $\text{Fe}^{3+}/(\text{Fe}^{3+} + \text{Si})$ of the structural units as a function of increasing $\text{Fe}^{3+}/(\text{Fe}^{3+} + \text{Si})$ of the system. Rather, tetrahedrally coordinated Fe^{3+} occurs in separate complexes which may or may not contain a fixed proportion of Si^{4+} . Thus, even though the scattering efficiency of individual $\text{Si}-\text{O}^-$ bonds in the quenched melts is somewhat dependent on the type of unit (Seifert et al., 1981), to a first approximation, the relative Raman band intensities (Table 4) may be used to indicate the trend of relative proportions of coexisting units as a function of iron content and temperature. This trend may then be used to indicate the changes in $-R\sum X_i \ln X_i$. Notably at 1550°C, the $E\eta^{\text{SW40F10}} / (E\eta^{\text{SW40F10}} + E\eta^{\text{SW40F5}}) = 0.58$. The ratio for the configurational entropy change [see equation (7) above] is 0.64. Thus, even with all these qualifying assumptions, the entropy ratio indicates a trend of $E\eta$ in the appropriate direction (activation energy decreases with increasing Fe_2O_3 content). In fact, the absolute value is off by only 15%. For the aluminous systems, the calculated values of $-R\sum X_i \ln X_i$ for both the A5 and A10 samples do

not vary significantly. The experimentally observed change in activation energy is within 10% (Fig. 4).

Data on melt structure of the compositions studied here are not available for other temperatures, but information from the system $\text{Na}_2\text{O}-\text{Al}_2\text{O}_3-\text{SiO}_2$ indicates that X_i (and, therefore $\sum X_i \ln X_i$) is dependent on both temperature and pressure (Mysen et al., 1985a). On the basis of the data in Figures 4 and 5 it is suggested that the temperature dependence of $-R\sum X_i \ln X_i$ is greater for iron-bearing than for aluminum-bearing samples because the activation energies of viscous flow of the iron-bearing samples are significantly temperature dependent [see also equation (4)]. Furthermore, one may conclude that $-R\sum X_i \ln X_i$ is less temperature dependent the more depolymerized the iron-bearing calcium silicate melts. The configurational entropy model appears, therefore, to relate melt structural data to activation energies of viscous flow. Limitations in available structural data preclude, however, a more detailed discussion at this time.

Acknowledgments

Critical reviews by Drs. J. Dickinson, T. Dunn, P. Richet and H. S. Yoder, Jr., are appreciated.

References

- Adam, G. and Gibbs, J. H. (1965) On the temperature dependence of cooperative relaxation properties in glass-forming liquids. *Journal of Chemical Physics*, 43, 139-146.
- Amthauer, G., Annersten, H. and Hafner, S. S. (1977) The Mössbauer spectrum of ^{57}Fe in titanium-bearing andradites. *Physics and Chemistry of Minerals*, 1, 399-413.
- Annersten, H. (1976) New Mössbauer data on iron in potash feldspar. *Neues Jahrbuch für Mineralogie, Abhandlungen*, 8, 337-343.
- Annersten, H. and Halenius, U. (1976) Iron distribution in pink muscovite: a discussion. *American Mineralogist*, 61, 1045-1050.
- Bockris, J. O'M. and Lowe, D. C. (1954) Viscosity and the structure of molten silicates. *Proceedings of the Royal Society*, 226A, 423-428.
- Bockris, J. O'M., Mackenzie, J. D. and Kitchner, J. A. (1955) Viscous flow in silicate and binary liquid silicates. *Transactions of the Faraday Society*, 51, 1734-1748.
- Cukiermann, M. and Uhlmann, D. R. (1974) Effect of iron oxidation state on viscosity, lunar composition 15555. *Journal of Geophysical Research*, 79, 1594-1598.
- Davidon, W. C. (1959) Variable metric method for minimization. AEC Research and Development Report ANL 5990. Argonne National Laboratory.
- Dickenson, M. P. and Hess, P. C. (1981) Redox equilibria and the structural role of iron in aluminosilicate melts. *Contributions to Mineralogy and Petrology*, 78, 352-358.
- Domine, F. and Piriou, B. (1983) Study of sodium silicate melt and glass by infrared reflectance spectroscopy. *Journal of Non-Crystalline Solids*, 55, 125-131.
- Fletcher, R. and Powell, M. J. D. (1963) A rapidly converging descent method for minimization. *Computer Journal*, 6, 163-168.
- Fox, K. E., Furukawa, T. and White, W. B. (1982) Transition metal ions in silicate melts. Part 2. Iron in sodium disilicate glasses. *Physics and Chemistry of Glasses*, 23, 169-178.

- Fulcher, G. S. (1925) Analysis of recent measurements of the viscosity of glasses. *American Ceramic Society Bulletin*, 8, 339–355.
- Furukawa, T., Fox, K. E. and White, W. B. (1981) Raman spectroscopic investigation of the structure of silicate glasses. III. Raman intensities and structural units in sodium silicate glasses. *Journal of Chemical Physics*, 75, 3226–3237.
- Hafner, S. S. and Huckenholz, H. G. (1971) Mössbauer spectrum of synthetic ferridiopside. *Nature (London), Physical Science*, 233, 255–261.
- Kozakevitch, P. (1960) Viscosité et éléments structuraux des aluminosilicates fondus: Laitiers CaO–Al₂O₃–SiO₂ entre 1600 and 2100°C. *Revue de Metallurgie (Paris)*, 51, 569–587.
- Klein, L. C., Fasano, B. V. and Wu, J. M. (1981) Flow behavior in ten iron-containing silicate compositions. *Proceedings of the 12th Lunar and Planetary Science Conference*, 1759–1767.
- Lacy, E. D. (1968) Structure transition in alkali silicate glasses. *Journal of the American Ceramic Society*, 51, 150–157.
- Lasaga, A. C. (1982) Optimization of CNDO for molecular orbital calculation on silicates. *Physics and Chemistry of Minerals*, 8, 36–46.
- Lazarev, A. N. (1972) *Vibrational Spectra and Structure of Silicates*. Consultants Bureau, New York.
- Mao, H. K., Virgo, D. and Bell, P. M. (1973) Analytical study of the orange soil returned by the Apollo 17 astronauts. *Carnegie Institution of Washington Year Book*, 72, 631–638.
- McMillan, P. and Piriou, B. (1983) Raman spectroscopic studies of silicate and related glass structure: a review. *Bulletin de Minéralogie*, 106, 57–77.
- McMillan, P., Piriou, B. and Navrotsky, A. (1982) A Raman spectroscopic study of glasses along the joins silica-calcium aluminate, silica-sodium aluminate and silica-potassium aluminate. *Geochimica et Cosmochimica Acta*, 46, 2021–2037.
- Mo, X., Carmichael, I. S. E., Rivers, M. and Stebbins, J. (1982) The partial molar volume of Fe₂O₃ in multicomponent silicate glasses and the pressure dependence of oxygen fugacity in magmas. *Mineralogical Magazine*, 45, 237–245.
- Murase, T. and McBirney, A. R. (1973) Properties of some common igneous rocks and their melts at high temperature. *Bulletin of the Geological Society of America*, 84, 3563–3592.
- Mysen, B. O. and Virgo, D. (1978) Influence of pressure, temperature and bulk composition on melt structures in the system NaAlSi₃O₈–NaFe³⁺Si₂O₆. *American Journal of Science*, 278, 1307–1322.
- Mysen, B. O. and Virgo, D. (1983) Effect of pressure on the structure of iron-bearing silicate melts. *Carnegie Institution of Washington Year Book*, 82, 321–325.
- Mysen, B. O. and Virgo, D. (1984) Raman spectra and structure of fluorine- and water-bearing silicate glasses and melts. In R. L. Snyder, Ed., *Advances in Materials Characterization II*. Plenum Press. In Press.
- Mysen, B. O., Seifert, F. A. and Virgo, D. (1980) Structure and redox equilibria of iron-bearing silicate melts. *American Mineralogist*, 65, 867–884.
- Mysen, B. O., Virgo, D. and Kushiro, I. (1981) The structural role of aluminum in silicate melts—a Raman spectroscopic study at 1 atmosphere. *American Mineralogist*, 66, 678–701.
- Mysen, B. O., Virgo, D. and Seifert, F. A. (1982a) The structure of silicate melts: implications for chemical and physical properties of natural magma. *Reviews of Geophysics*, 20, 353–383.
- Mysen, B. O., Finger, L. W., Seifert, F. A. and Virgo, D. (1982b) Curve-fitting of Raman spectra of amorphous solids. *American Mineralogist*, 67, 686–696.
- Mysen, B. O., Virgo, D. and Seifert, F. A. (1982c) Distribution of aluminum between anionic units in depolymerized silicate melts as a function of pressure and temperature. *Carnegie Institution of Washington Year Book*, 81, 360–366.
- Mysen, B. O., Virgo, D. and Seifert, F. A. (1984) Redox equilibria of iron in alkaline earth silicate melts: relationship between melt structure, oxygen fugacity, temperature and properties of iron-bearing silicate liquids. *American Mineralogist*, 69, 834–847.
- Mysen, B. O., Virgo, D. and Seifert, F. A. (1985a) Relationships between properties and structure of aluminosilicate melts. *American Mineralogist*, 70, 88–105.
- Mysen, B. O., Virgo, D., Neumann, E.-R. and Seifert, F. A. (1985b) Redox equilibria and the structural states of ferric and ferrous iron in melts in the system CaO–MgO–Al₂O₃–SiO₂–Fe–O: Relationships between redox equilibria, melt structure and liquidus phase equilibria. *American Mineralogist*, 70, 317–331.
- Navrotsky, A., Peraudeau, M., McMillan, P. and Coutoures, J.-P. (1982) A thermochemical study of glasses and crystals along the joins silica-calcium aluminate and silica sodium aluminate. *Geochimica et Cosmochimica Acta*, 46, 2039–2049.
- Nolet, D. A., Burns, R. G., Flamm, S. L. and Besancon, J. R. (1979) Spectra of Fe-Ti silicate glasses: implications to remote-sensing of planetary surfaces. *Proceedings of the 10th Lunar and Planetary Science Conference*, 10, 1775–1786.
- Osborn, E. F. and Muan, A. (1960a) Phase equilibrium diagrams of oxide systems. Plate 10. The system CaO–Fe₂O₃–SiO₂. *American Ceramic Society*, Columbus, Ohio.
- Osborn, E. F. and Muan, A. (1960b) Phase equilibrium diagrams of oxide systems. Plate 2. The system CaO–Al₂O₃–SiO₂. *American Ceramic Society*, Columbus, Ohio.
- Powell, M. J. D. (1964a) An efficient method for finding the minimum of a function of several variables without calculating derivatives. *Computer Journal*, 7, 155–162.
- Powell, M. J. D. (1964b) A method for minimizing a sum of squares of non-linear functions without calculating derivatives. *Computer Journal*, 7, 303–307.
- Richert, P. (1984) Viscosity and configurational entropy of silicate melts. *Geochimica et Cosmochimica Acta*, 48, 471–485.
- Riebling, E. F. (1964) Structure of magnesium aluminosilicate liquids at 1700°C. *Canadian Journal of Chemistry*, 42, 2811–2821.
- Riebling, E. F. (1966) Structure of sodium aluminosilicate melts containing at least 50 mole% SiO₂ at 1500°C. *Journal of Chemical Physics*, 44, 2857–2865.
- Rontgen, P., Winterhager, H. and Kammel, R. (1956) Struktur und Eigenschaften von Schlacken der Metallhüttenprozesse. I. Viskositätsmessungen an Schlacken des Systems Eisenoxydul-Tonerde-Kieselsäure. *Zeitschrift für Erzbergbau und Metallhüttenwesen*, 5, 207–214.
- Rontgen, H., Winterhager, P. and Kammel, R. (1960) Struktur und Eigenschaften von Schlacken der Metallhüttenprozesse. II. Viskositätsmessungen an Schmelzen der System Eisenoxydul-Kalk-Kieselsäure und Eisenoxydul-Kalk-Tonerde-Kieselsäure. *Zeitschrift für Erzbergbau und Metallhüttenwesen*, 8, 363–373.
- Rossin, R., Berson, J. and Urbain, G. (1964) Etude de la viscosité de laitiers liquides appartenant au système ternaire: SiO₂–Al₂O₃–CaO. *Revue des Hautes Températures et des Refractaires*, 1, 159–170.
- Sack, R. O., Carmichael, I. S. E., Rivers, M. and Ghiorsio, M. S. (1980) Ferric-ferrous equilibria in natural silicate liquids at 1 bar. *Contributions to Mineralogy and Petrology*, 75, 369–377.
- Scarfe, C. M. (1973) Viscosity of basic magmas at varying pressure. *Nature (London), Physical Science*, 241, 101–102.
- Scarfe, C. M. (1977) Viscosity of a pantellerite melt at one atmosphere. *Canadian Mineralogist*, 15, 185–189.

- Scarfe, C. M., Cronin, D. J., Wenzel, J. T. and Kaufmann, D. A. (1983) Viscosity-temperature relationships at 1 atm in the system diopside-anorthite. *American Mineralogist*, 68, 1083-1089.
- Seifert, F. A. and Olesch, M. (1977) Mössbauer spectroscopy of grandidierite, $(\text{Mg,Fe})\text{Al}_3\text{BSiO}_9$. *American Mineralogist*, 62, 547-553.
- Seifert, F. A., Mysen, B. O. and Virgo, D. (1981) Quantitative determination of proportions of anionic units in silicate melts. *Carnegie Institution of Washington Year Book*, 80, 301-302.
- Seifert, F. A., Mysen, B. O. and Virgo, D. (1982) Three-dimensional network melt structure in the systems SiO_2 - NaAlO_2 , SiO_2 - CaAl_2O_4 and SiO_2 - MgAl_2O_4 . *American Mineralogist*, 67, 696-718.
- Shaw, H. R. (1960) Rheology of basalt in the melting range. *Journal of Petrology*, 10, 510-535.
- Tarte, P., Pottier, M. J. and Proce, A. M. (1973) Vibrational studies of silicates and germanates. V. Infrared and Raman spectra of pyrosilicates and pyrogermanates with linear bridge. *Spectrochimica Acta*, 29A, 1017-1027.
- Taylor, M. and Brown, G. E. (1979a) Structure of mineral glasses. I. The feldspar glasses $\text{NaAlSi}_3\text{O}_8$, KAlSi_3O_8 and $\text{CaAl}_2\text{Si}_2\text{O}_8$. *Geochimica et Cosmochimica Acta*, 43, 61-77.
- Taylor, M. and Brown, G. E. (1979b) Structure of mineral glasses. II. The SiO_2 - NaAlSiO_4 join. *Geochimica et Cosmochimica Acta*, 43, 1467-1475.
- Toop, G. W. and Samis, C. S. (1962) Activities of ions in silicate melts. *Transactions of the American Institute of Mining Engineers*, 224, 878-887.
- Verweij, H. (1979a) Raman study of the structure of alkali germanosilicate glasses. I. Sodium and potassium metagermanosilicate glasses. *Journal of Non-Crystalline Solids*, 33, 41-53.
- Verweij, H. (1979b) Raman study of the structure of alkali germanosilicate glasses. II. Lithium, sodium and potassium digermanosilicate glasses. *Journal of Non-Crystalline Solids*, 33, 55-69.
- Virgo, D., Mysen, B. O., Danckwerth, P. A. and Seifert, F. A. (1982) Speciation of Fe^{3+} in 1-atm Na_2O - SiO_2 - Fe-O melts. *Carnegie Institution of Washington Year Book*, 81, 349-353.
- Virgo, D., Mysen, B. O. and Danckwerth, P. A. (1983) Redox equilibria and the anionic structure of $\text{Na}_2\text{O} \cdot x\text{SiO}_2$ - Fe-O melts: effects of oxygen fugacity. *Carnegie Institution of Washington Year Book*, 82, 305-309.
- Waychunas, G. A. and Rossman, F. R. (1983) Spectroscopic standard for tetrahedrally coordinated ferric iron: $\gamma\text{LiAlO}_2:\text{Fe}^{3+}$. *Physics and Chemistry of Minerals*, 9, 212-215.

*Manuscript received, April 26, 1984;
accepted for publication, January 15, 1985.*